

Carbon nanotube as a Cherenkov-type light emitter and free electron laser

K. G. Batrakov, S. A. Maksimenko, and P. P. Kuzhir

Institut für Nuclear Problems, Belarus State University, Bobruiskaya 11, 220050 Minsk, Belarus

C. Thomsen

Institut für Festkörperphysik, Technische Universität Berlin, Hardenbergstr. 36, D-10623 Berlin, Germany

(Received 18 July 2008; published 5 March 2009)

A mechanism of stimulated emission of electromagnetic radiation by an electron beam in carbon nanotubes is theoretically considered. Three basic properties of carbon nanotubes: a strong slowing down of surface electromagnetic waves, ballisticity of the electron motion over typical nanotube length, and extremely high electron current density reachable in nanotubes, allow proposition of them as candidates for the development of nanoscale Cherenkov-type emitters, analogous to traveling-wave tube and free electron laser. Dispersion equations of the electron-beam instability and the threshold conditions of the stimulated emission have been derived and analyzed, demonstrating realizability of the nanotube-based nano-free electron lasers at realistic parameters of nanotubes and electronic beams.

DOI: [10.1103/PhysRevB.79.125408](https://doi.org/10.1103/PhysRevB.79.125408)

PACS number(s): 41.60.-m, 78.67.Ch, 73.63.Fg

I. INTRODUCTION

Since the discovery of carbon nanotubes (CNTs) in 1991,¹ there has been great interest to their outstanding structural, electrical, and mechanical properties^{2,3} due to wide applications ranging from chemical and biological sensors and actuators to field emitters to mechanical fillers for composite materials. Among others, the study of CNTs as building blocks for nanoelectronics⁴ and nano-optics⁵ has continued to grow unabated owing to the great potentiality for the miniaturization and the increase in operational speed of optoelectronic nanocircuits, and for the use in near-field sub-wavelength optical element. In that relation, the question of electromagnetic response properties of CNTs arises. Many interesting physical effects have been revealed, such as excitation of surface plasmons,⁶ guiding of strongly slowed-down electromagnetic surface waves,^{7,8} antenna effect-controlled and enhanced radiation efficiency in infrared and terahertz ranges,⁹⁻¹³ enhanced spontaneous decay rate of an excited atom in the vicinity of CNT,¹⁴ and formation of the discrete spectrum in thermal radiation of finite-length metallic CNTs in the terahertz range.¹⁵ Recently, nanoscale optical imaging of single-walled CNTs has been studied by means of high-resolution near-field Raman microscopy,^{16,17} and antenna operation of a CNT array has been demonstrated experimentally.¹⁸ Reference 19 reports multiwall CNT as subwavelength coaxial waveguide for visible light.

An intriguing problem of nanoelectromagnetism is the development of CNT-based nanoscale sources of light. A mechanism of the emission of hard x radiation by a charged particle moving in a CNT has been considered in Ref. 20. The use of CNTs in x-ray and high-energy particle optics as focusing and guiding elements, and as x-ray sources is presently discussed.^{21,22} In the optical range, the mechanism of light emission due to exciton recombination in semiconductor CNTs has been proposed and experimentally verified.^{23,24} In line with the present-day tendency of the terahertz frequency range exploration and exploitation,²⁵ a possibility of terahertz emission in CNTs imposed to transverse and axial electric fields due to electric-field induced heating of electron

gas has been investigated.²⁶⁻³⁰ Recently, the idea using kinetic energy of CNT-guided electron beam for stimulated emission of electromagnetic waves in optical and terahertz ranges has been proposed.³¹⁻³⁴ In the given paper we present a consistent theory of the effect.

There is a wide family of devices utilizing interaction of electron beams with electromagnetic waves to produce electromagnetic radiation. Started by the invention of klystrons,³⁵ this family embraces such well-known systems as traveling-wave tubes (TWT), backward wave oscillators (BWO),³⁶ free electron lasers (FEL),³⁷⁻⁴⁰ etc. In systems of that kind, synchronous motion of electrons and electromagnetic wave modulates the electron beam, and coherent radiation is produced by electron bunches. The radiation frequency is smoothly tunable due to its dependence on the electron-beam energy. Therefore, such type of emitters can operate in wide spectral range from microwave and infrared frequencies to vacuum ultraviolet nowadays (e.g., VUV-FEL at DESY). Several projects aimed with the lasing in hard x-ray range have started.^{41,42}

The synchronization of moving electrons and electromagnetic wave is attained either by slowing down the electromagnetic wave (Cherenkov, Smith-Purcell,⁴³ and quasi-Cherenkov⁴⁴ radiation mechanisms) or by applying an external magnetic field, which is uniform in gyrotrons^{45,46} and spatially periodical in undulators.³⁹ Besides, the oscillator-type mechanism⁴⁷ is realized for electrons with discrete spectrum of transverse motion (for example, for electron channeling in crystals). The Cherenkov radiation is governed by the synchronization condition $\omega - \mathbf{k}\mathbf{u} = 0$, where \mathbf{k} is the wave vector and \mathbf{u} is the charged particle (electron) velocity. In systems with external fields the synchronism condition is transformed to $\omega - \mathbf{k}\mathbf{u} - \Omega = 0$ with Ω as the electron oscillation frequency. In the oscillator regime Ω is the transition frequency between electron levels.⁴⁸

For the coherent generation in the devices described, a high vacuum must be maintained in the region of the electron-beam–electromagnetic wave interaction.⁴⁹ Otherwise, collisions of electrons with atoms move electrons out of the synchronism and, consequently, lasing is not reached.

From this point of view CNTs are unique objects since they exhibit ballistic electrical conduction at room temperature with mean-free paths on the order of microns and even tens of microns.^{50–52} Therefore, electrons can emit coherently from the whole CNT length which is typically 1–10 μm . Besides, single-walled and multiwalled carbon nanotubes can carry a high current density of the order of $10^9\text{--}10^{10}$ A/cm², see, e.g., Refs. 53–55. Lastly, metallic CNTs exhibit a strong, as large as 50–100 times, slowing down of surface electromagnetic waves.^{7,8} Thus, a combination in CNTs of three key properties: (i) ballisticity of the electron flow over typical CNT length, (ii) extremely high current-carrying capacity, and (iii) strong slowing down of surface electromagnetic waves, allows proposition of them as candidates for the development of nanosized Cherenkov-type emitters—nano-TWT, nano-BWO, and nano-FEL. Note that practical realization of the idea in single-walled CNTs will meet the problem of the ballisticity retaining at high current density. Some possible ways to get over the problem are discussed below in Sec. IV.

The remainder of the paper is organized as follows. In Sec. II we derive dispersion equation for electromagnetic wave coupled with electron beam, and discuss its solution in classical and quantum limits. A solution of the boundary-value problem for a finite-length CNT is presented in Sec. III allowing evaluation of the absolute instability gain and the lasing threshold currents. Section IV contains physical analysis of the results obtained and numerical estimates for the gain and threshold currents. Concluding remarks are given in Sec. V.

II. RADIATIVE INSTABILITY OF ELECTRON BEAM IN CARBON NANOTUBE

A. Self-consistent equation of motion for electromagnetic wave and electron beam

Nanotubes—quasi-one-dimensional carbon macromolecules—are obtained by rolling up graphene layer into a cylinder. The transformation can be performed in different manners classified by the dual index (n_1, n_2) . The two integers n_1 and n_2 represent the vector characterizing the way of turning, with $n_1=0$ for zigzag CNTs, $n_1=n_2$ for armchair CNTs, and $0 < n_1 \neq n_2$ for chiral CNTs. A nanotube can manifest either metallic or semiconductor properties, depending on its radius R_{cn} and the direction of rolling up. This correlation arises from the transverse quantization of charge-carrier motion and is due to the quasi-one-dimensional topology of CNTs; for details see, e.g., Refs. 2 and 3.

Consider an electron beam moving in an isolated single-walled carbon nanotube oriented along the z axis. The electron beam can be injected into the nanotube from outside by an external source or can be produced by applying voltage to some section of the nanotube. Accelerated by the voltage, electrons are injected into the working region. Independently on the origin of electrons, their motion in this region is assumed to be ballistic.

As was mentioned in Sec. I, there is a certain analogy between a CNT guiding electron beam and macroscopic vacuum electron devices. The main (and obvious) distinction

is the small cross-sectional radius of CNTs as compared to their macroscopic analogs. As a result, in CNTs spatial quantization of the electron motion comes into play and, therefore, classical models of the electron beam become inapplicable. The electron motion in CNTs is governed by quantum-mechanical equations. In this paper we shall consider the lasing effect when the generated field is rather large, i.e., the condition

$$E \gg \sqrt{\hbar}c \left(\frac{\omega}{c} \right)^2 \quad (1)$$

is fulfilled.⁵⁶ In this case the electromagnetic wave has classical character and is described by the classical wave equation:

$$\nabla \nabla \cdot \mathbf{E}(\mathbf{r}, \omega) - \Delta \mathbf{E}(\mathbf{r}, \omega) = \frac{4\pi i \omega}{c^2} \mathbf{j}(\mathbf{r}, \omega). \quad (2)$$

If condition (1) does not hold, the number of photons per quantum level becomes too small to apply a classical approach and the electromagnetic field must be considered within the quantum electrodynamics. The quantum-electrodynamical consideration is of importance on the initial stage of the instability development, when few photons participate in the process. We leave this stage for further analysis to focus on the stage of highly developed instability. Thus, in our model the electron motion is governed by the Schrödinger equation while the electromagnetic field is described by classical Maxwell equations. In the right-hand part of field Eq. (2) the quantity $\mathbf{j}(\mathbf{r}, \omega)$ is the current density averaged over the quantum states of the electron beam.

The current density in the working region is defined by the well-known equation:⁵⁷

$$\begin{aligned} \mathbf{j}(\mathbf{r}, t) = & \frac{e}{2m_e} \{ \psi^*(\mathbf{r}, t) \hat{\mathbf{p}} \psi(\mathbf{r}, t) - [\hat{\mathbf{p}} \psi^*(\mathbf{r}, t)] \psi(\mathbf{r}, t) \} \\ & - \frac{e^2}{m_e c} |\psi(\mathbf{r}, t)|^2 \mathbf{A}(\mathbf{r}, t). \end{aligned} \quad (3)$$

Here $\hat{\mathbf{p}} = -i\hbar \partial / (\partial \mathbf{r})$ is the momentum operator and $\mathbf{A}(\mathbf{r}, t)$ is the vector potential of electromagnetic field. Further we neglect the Fermi law for the electron statistics. This is possible because the number of excited electrons per quantum level is found to be small even at superior current densities reachable in CNTs.^{53–55} Indeed, the number of levels in the interaction volume V is estimated as $\sim V p^3 / (2\pi\hbar)^3$, where p is a typical value of quasimomentum of electrons in the beam. The number of electrons in this volume is $\sim n_e V$, where n_e is the electron density. Then, the number of excited electrons per level is given by $\eta_e = (2\pi\hbar)^3 n_e / p^3$. At current density of $10^8\text{--}10^{10}$ A/cm² and an excitation energy of the order of several electron volts, we find $\eta_e \sim 10^{-5}\text{--}10^{-3}$. Therefore, the exchange interaction between electrons in the beam can be neglected.

Let $\psi(\mathbf{r}, t=0) = \psi_n(\mathbf{r})$ be the eigenfunction of an electron noninteracting with electromagnetic wave and moving along the CNT. When the interaction is switched on, the wave function is represented by the expansion

$$\psi(\mathbf{r}, t) = \sum_l a_l(t) \exp(-i\varepsilon_l t/\hbar) \psi_l(\mathbf{r}) \quad (4)$$

over a complete set of the unperturbed eigenfunctions $\psi_l(\mathbf{r})$ with ε_l as corresponding energy eigenvalues. For further convenience, we rewrite the coefficients $a_l(t)$ as $a_l(t) = \delta_{ln} + \delta a_l^{(n)}(t)$, where δ_{ln} is the Kronecker symbol. Corrections $\delta a_l^{(n)}(t)$ are due to the electron–electromagnetic field interaction. Taking into account axial periodicity of the nanotube potential, the wave functions $\psi_l(\mathbf{r})$ can be written in accordance with the Bloch theorem as

$$\psi_l(\mathbf{r}) = \exp\{ip_l z/\hbar\} \sum_{\tau} b_{l\tau} \exp\{i\tau z\} u_{l\tau}(\mathbf{r}_{\perp}). \quad (5)$$

Here p_l is the axial projection of the quasimomentum of l th state, $b_{l\tau}$ are constant coefficient, $\tau = 2\pi q/a$ are the reciprocal-lattice constants, a is the CNT spatial period in the axial direction, $u_{l\tau}(\mathbf{r}_{\perp})$ are functions dependent only on transverse coordinates, and q are integers. The term $\sum_{\tau} b_{l\tau} \exp\{i\tau z\} u_{l\tau}(\mathbf{r}_{\perp})$ is periodical in the z direction.

In linear approximation, the contribution to electron current (3) originated from the electron–electromagnetic field interaction is described by the equation:

$$\begin{aligned} \delta \mathbf{j}_n(\mathbf{r}, t) = & \frac{e}{2m_e} \sum_l \{ \delta a_l^{(n)*}(t) \exp[i(\varepsilon_l - \varepsilon_n)t/\hbar] \{ \psi_l^*(\mathbf{r}) \hat{\mathbf{p}} \psi_n(\mathbf{r}) \\ & - [\hat{\mathbf{p}} \psi_l^*(\mathbf{r})] \psi_n(\mathbf{r}) \} + \delta a_l^{(n)}(t) \exp[-i(\varepsilon_l - \varepsilon_n)t/\hbar] \\ & \times \{ \psi_n^*(\mathbf{r}) \hat{\mathbf{p}} \psi_l(\mathbf{r}) - [\hat{\mathbf{p}} \psi_n^*(\mathbf{r})] \psi_l(\mathbf{r}) \} \} \\ & - \frac{e^2}{m_e c} |\psi_n|^2 \mathbf{A}(\mathbf{r}, t). \end{aligned} \quad (6)$$

Then, applying to Schrödinger equation standard perturbation-theory technique,⁵⁷ we obtain the equation describing the dynamics of the coefficients $\delta a_l(t)$:

$$\begin{aligned} i\hbar \sum_l \frac{\partial \delta a_l^{(n)}(t)}{\partial t} \psi_l(\mathbf{r}) \exp(-i\varepsilon_l t/\hbar) \\ = - \frac{e}{2m_e c} \times [\mathbf{A}(\mathbf{r}, t) \hat{\mathbf{p}} + \hat{\mathbf{p}} \mathbf{A}(\mathbf{r}, t)] \psi_n(\mathbf{r}) \exp(-i\varepsilon_n t/\hbar), \end{aligned} \quad (7)$$

which is obtained by substitution of Eq. (4) into the Schrödinger equation and its subsequent linearization with respect to the electromagnetic field strength. The Fourier transform of Eq. (7) gives

$$\begin{aligned} \delta a_l^{(n)}(\omega) = & \frac{e}{2m_e \omega \hbar c} \langle l | \mathbf{A} \left(\mathbf{r}, \omega + \frac{\varepsilon_l - \varepsilon_n}{\hbar} \right) \hat{\mathbf{p}} \\ & + \hat{\mathbf{p}} \mathbf{A} \left(\mathbf{r}, \omega + \frac{\varepsilon_l - \varepsilon_n}{\hbar} \right) | n \rangle. \end{aligned} \quad (8)$$

Here we use the standard ket and bra notation of wave functions and matrix elements, $|l\rangle = \psi_l(\mathbf{r})$. Only those terms are preserved in Eq. (8) which corresponds to resonant interaction between electrons and electromagnetic field. Contribution of the last term in Eq. (6) is therefore neglected in Eq. (8). Performing the Fourier transform of Eq. (6) along the

axial coordinate and time, we come to the k, ω -space interaction-induced current-density correction:

$$\begin{aligned} \delta \mathbf{j}_n(k, \mathbf{r}_{\perp}, \omega) = & - \frac{e^2}{4m_e^2 c} \sum_l B_{nl}(k, \mathbf{r}_{\perp}, \omega) \sum_{\tau' \tau} \\ & \times \left\{ - \frac{b_{l\tau'}^* b_{n\tau} [u_{l\tau'}^*(\hat{\mathbf{p}}_n + \boldsymbol{\tau}) + (\hat{\mathbf{p}}_n + \boldsymbol{\tau}) u_{l\tau'}^*] u_{n\tau}}{\hbar \omega + \varepsilon_l(p_n - k) - \varepsilon_n(p_n)} \right. \\ & \left. + \frac{b_{n\tau}^* b_{l\tau'} [u_{n\tau}^*(\hat{\mathbf{p}}_n + \boldsymbol{\tau}) + (\hat{\mathbf{p}}_n + \boldsymbol{\tau}) u_{n\tau}^*] u_{l\tau'}}{\hbar \omega + \varepsilon_n(p_n) - \varepsilon_l(p_n + k)} \right\}. \end{aligned} \quad (9)$$

For convenience, we have introduced the vector form for the lattice constant $\boldsymbol{\tau} = \tau \mathbf{e}_z$, where \mathbf{e}_z is the unit axial vector. The quasimomentum operator in matrix elements is given by $\hat{\mathbf{p}}_n = \{\hat{\mathbf{p}}_{\perp}, p_n\}$, where axial components p_n are C numbers and transverse components $\hat{\mathbf{p}}_{\perp}$ are operators. These operators act only on the right-adjacent functions. Deriving Eq. (9), we neglect the longitudinal component k of the electromagnetic wave vector in matrix elements since $\hbar k/p_n \ll 1$. Summation over the lattice constants τ and τ' is not independent: for every τ in sum, the value of τ' must be such that the values $p_n + \tau - \tau'$ are in the first Brillouin zone. The coefficients $B_{nl}(k, \mathbf{r}_{\perp}, \omega)$ are given by

$$\begin{aligned} B_{nl}(k, \mathbf{r}_{\perp}, \omega) = & \sum_{\tau' \tau} b_{l\tau'} b_{n\tau}^* \langle u_{n\tau} | (\hat{\mathbf{p}}_n + \boldsymbol{\tau}) \mathbf{A}(k, \mathbf{r}_{\perp}, \omega) \\ & + \mathbf{A}(k, \mathbf{r}_{\perp}, \omega) (\hat{\mathbf{p}}_n + \boldsymbol{\tau}) | u_{l\tau'} \rangle. \end{aligned}$$

Substituting then Eq. (9) into Eq. (2), we come to a self-consistent field equation necessary for the further analysis.

B. Dispersion equation for electromagnetic wave coupled with electron beam

Electromagnetic response properties of an isolated single-walled CNT was studied in Ref. 7 on the base of a tight-binding microscopic model of the CNT conductivity and the effective boundary conditions for electromagnetic field imposed on the CNT surface. A detailed analysis of the eigen-wave problem has revealed propagation in CNT strongly slowed-down surface waves allowing the concept of nanotubes as surface-wave nanowaveguides. Considering the electron beam as a perturbation, we can use the dispersion equation for the surface waves and the propagation constants obtained in Ref. 7 as a zero-order approximation. Then, the self-consistent field of the electromagnetic wave coupled with electron beam can be presented by the expansion

$$\mathbf{A}(k, \mathbf{r}_{\perp}, \omega) = \sum_m \alpha_m(k, \omega) \mathbf{A}_m(\mathbf{r}_{\perp}), \quad (10)$$

where vector potentials $\mathbf{A}_m(\mathbf{r}_{\perp})$ correspond to the electromagnetic field eigenfunctions evaluated in Ref. 7 and $\alpha_m(k, \omega)$ are the coefficients to be found. Substitution of Eqs. (6), (9), and (10) into Eq. (2) gives the system of equations for the electromagnetic field interacting with the electrons occupying n th state:

$$\begin{aligned}
 & \sum_m (k^2 - k_m^2) \alpha_m(k, \omega) \mathbf{A}_m(\mathbf{r}_\perp) \\
 &= -\frac{4\pi}{c} \frac{e^2 n_e}{4m_e^2 c} \sum_l B_{nl}(k, \mathbf{r}_\perp, \omega) \sum_{\tau, \tau'} \\
 & \times \left\{ -\frac{b_{l\tau'}^* b_{n\tau} [u_{l\tau'}^* (\hat{\mathbf{p}}_n + \boldsymbol{\tau}) + (\hat{\mathbf{p}}_n + \boldsymbol{\tau}) u_{l\tau'}^*] u_{n\tau}}{\hbar\omega + \varepsilon_l(p_n - k) - \varepsilon_n(p_n)} \right. \\
 & \left. + \frac{b_{n\tau}^* b_{l\tau'} [u_{n\tau}^* (\hat{\mathbf{p}}_n + \boldsymbol{\tau}) + (\hat{\mathbf{p}}_n + \boldsymbol{\tau}) u_{n\tau}^*] u_{l\tau'}}{\hbar\omega + \varepsilon_n(p_n) - \varepsilon_l(p_n + k)} \right\}. \quad (11)
 \end{aligned}$$

Here k_m are the wave numbers corresponding to the physical system devoid electron beam. As one can see, deriving Eq. (11) we have proceeded from the single-electron dynamics to the dynamics of the electron beam: n_e is the electron density. Multiplying left-hand and right-hand parts of Eq. (11) by $\mathbf{A}_m^*(\mathbf{r}_\perp)$ and utilizing the wave functions' orthogonality, we come to the dispersion equation as follows:

$$\begin{aligned}
 k - k_m = & -\frac{\omega_L^2}{8k_m m_e c^2} \sum_l |B_{nl}^{(m)}|^2 \\
 & \times \left[\frac{1}{-\hbar\omega + \varepsilon_n(p_n) - \varepsilon_l(p_n - k)} \right. \\
 & \left. + \frac{1}{\hbar\omega + \varepsilon_n(p_n) - \varepsilon_l(p_n + k)} \right]. \quad (12)
 \end{aligned}$$

The upper index in $B_{nl}^{(m)}$ relates the matrix element with the corresponding mode of the electromagnetic field $\mathbf{A}_m(\mathbf{r}_\perp)$; $\omega_L = 2\sqrt{\pi e^2 n_e / m_e}$ is the Langmuir frequency of the electron beam.

Transcendent dispersion Eq. (12) predicts the existence of a variety of branches of wave number k . Among them, the number of branches to be accounted for is defined by specific physical parameters of analyzed system. In the vicinity of a resonance, only terms corresponding to the resonant interaction, one or several (in the case of level degeneration) can be kept in the dispersion equation. If the difference between levels exceeds the linewidth, only the resonant term is of importance.

C. Classical and quantum limits in synchronism conditions

Two terms in the right-hand part of Eq. (12) dictate two synchronism conditions corresponding to the resonant interaction between electron beam and electromagnetic wave:

$$\pm \hbar\omega + \varepsilon_n(p_n) - \varepsilon_l(p_n \pm k) = 0. \quad (13)$$

The signs “+” and “-” correspond to the absorption and the emission of photon by electron, respectively. Dependently on the relation between electron and photon energies, different interaction regimes are realized. As we restricted ourselves to the case when the photon momentum is much less than the electron one, the electron energy $\varepsilon_l(p_n \pm \hbar k)$ can be presented by the truncated Taylor series as

$$\varepsilon_l(p_n \pm \hbar k) = \varepsilon_l(p_n) \pm \hbar k \frac{\partial \varepsilon_l(p_n)}{\partial p_n} \equiv \varepsilon_l(p_n) \pm \hbar k v_l,$$

where v_l is the electron group velocity. Then, denominators in Eq. (12) can be represented by

$$\begin{aligned}
 & \pm \hbar\omega + \varepsilon_n(p_n) - \varepsilon_l(p_n \pm k) \approx \pm \hbar(\omega - k v_l \pm \Omega_{nl}) \\
 & + \frac{\hbar^2}{2} \frac{\partial^2 \varepsilon_l}{\partial p_n^2} k^2. \quad (14)
 \end{aligned}$$

The first term in the right-hand part of this equation is analogous to the standard term $\omega - k v \pm \Omega$ in the synchronism condition.⁴⁷ The only difference is that the velocity of free electrons is replaced by the group velocity of quasielectrons v_l and the undulation frequency is replaced by the transition frequency $\Omega_{nl} = [\varepsilon_n(p_n) - \varepsilon_l(p_n)] / \hbar$ between CNT energy bands. The last term in Eq. (14) originates from the quantum recoil of electron during emission (absorption) of photon and induces a redshift (blueshift) of the transition frequency. This term is inversely proportional to the electron effective mass (second derivative of the energy). Let $l=s$ be an electron level corresponding to the resonant interaction. Then, within the approximation stated, the dispersion equation takes the form as follows:

$$k - k_m = \frac{\frac{2}{\hbar} b_{ns}^{(m)} \left(\frac{\hbar k^2}{2} \frac{\partial^2 \varepsilon_s}{\partial p_n^2} - \Omega_{ns} \right)}{(\omega - k v_s)^2 - \left(\frac{\hbar k^2}{2} \frac{\partial^2 \varepsilon_s}{\partial p_n^2} - \Omega_{ns} \right)^2}, \quad (15)$$

where

$$b_{ns}^{(m)} = -\frac{\omega_L^2 \hbar}{8m_e k_m' c^2} |B_{ns}^{(m)}|^2, \quad k_m' = \text{Re}(k_m).$$

In the case of intraband transitions, $\Omega_{ns} = 0$ and Eq. (15) takes the form of the dispersion equation for the instability with the recoil accounted for.³⁷

Depending on ratio between the radiation linewidth and the recoil-induced detuning, two different generation regimes are realized. In the low-gain limit³⁹ the spontaneous emission linewidth can be estimated as $\Delta\omega / \omega \sim c / (\omega L)$, where L is the interaction length. If the linewidth exceeds the recoil energy, the recoil term in the denominator of Eq. (15) can be neglected and the classical interaction regime is realized. The dispersion equation in that case takes the traditional form of the second-order Cherenkov resonance:

$$k - k_m = k^2 \frac{\partial^2 \varepsilon_s}{\partial p_n^2} \frac{b_{ns}^{(m)}}{(\omega - k v_s)^2}. \quad (16)$$

The *spatial increment* of the instability $k'' = \text{Im}(k)$ can be estimated using the method of weakly coupled modes.⁵⁸ According to this method, interaction between the electromagnetic wave and the electron beam is essential only in the vicinity of the point $(\omega_0, k_0 = \omega_0 / v_s)$ where the dispersion curves of noninteracting modes, $\omega - k v_s = 0$ and $k(\omega) = k_m(\omega)$, are crossed. Then k_m is represented by the expansion

$$k_m(\omega) = k_0 + \left. \frac{\partial k_m(\omega)}{\partial \omega} \right|_{\omega=\omega_0} (\omega - \omega_0). \quad (17)$$

Substitution of this expansion and $k=k_0+\Delta k$ into Eq. (16) results in a third-order algebraic equation with respect to Δk . From this equation, the instability spatial increment is estimated at the frequency $\omega=\omega_0$ as

$$|\Delta k''| = \frac{\sqrt{3}}{2} \left| b_{nn}^{(m)} \frac{\partial^2 \varepsilon_n}{\partial p_n^2} \frac{k^2}{v_n^2} \right|^{1/3}, \quad (18)$$

where $\Delta k'' = \text{Im}(\Delta k)$. Since $b_{nn} \sim n_e$, the increment is found to be the third root of the electron density. Such a dependence is typical for the Compton-type radiative instability.³⁹

In the opposite case, when the linewidth is less than the difference between the emission and the absorption frequencies, we fall into regime of the *strong quantum recoil impact*. In this case, only the term corresponding to the emission survives in dispersion Eq. (12), which therefore is reduced to

$$k - k_m = \frac{b_{nn}^{(m)}}{\hbar} \frac{1}{\omega - v_s k - \frac{\hbar}{2} \frac{\partial^2 \varepsilon_n}{\partial p_n^2} k^2}. \quad (19)$$

As a result, the instability increment is given by

$$|\Delta k''| = \left| \frac{b_{nn}^{(m)}}{\hbar v_n} \right|^{1/2}, \quad (20)$$

i.e., turns out to be proportional to the square root of the electron density.

Below we present a detailed discussion of the different generation regimes and give some numerical estimates of physical parameters corresponding to these regimes.

III. STARTING CURRENTS AND THEIR DEPENDENCE ON THE NANOTUBE LENGTH

A. Boundary conditions for a finite-length nanotube

In Secs. II B and II C, dispersion equations have been derived providing us with wave-number eigenvalues in an infinite-length CNT guiding electron beam. As a next step, the system must be imposed by edge conditions accounting for the finite length of the interaction zone. These conditions are stated as the requirement to perturbations of the electron and current densities, generated by the electron-beam–electromagnetic wave interaction, to be zero at the input of the working zone, i.e.,

$$\delta n_e(z=0) = \delta j_n(z=0) = 0. \quad (21)$$

The condition that the tangential electric-field component and the axial component of the magnetic field be continuous on the CNT surface yields additional boundary condition. We write it in the simplified form⁵⁹ as

$$E(z=0) = \alpha E(z=L), \quad (22)$$

where α is the reflection coefficient of electromagnetic field from the working zone boundaries.

The field distribution in a finite-length system consisting of several parts can be found by solving electrodynamic

problem in each region separately and then joining the solutions by means of boundary conditions. In the interaction region, the electromagnetic field is given by

$$E(z) \sim \sum_{i=1}^N c_i \exp(ik^{(i)}z), \quad (23)$$

where the summation is performed over all electromagnetic modes in CNT; the wave numbers $k^{(i)}$ are determined by corresponding dispersion equations. Note that the reflection of electromagnetic waves from boundaries back into the working zone creates positive feedback in the system, and thus allows accumulation of the electromagnetic energy and provides an oscillator regime.

B. Starting current at a large quantum recoil

In the quantum interaction regime, when the quantum recoil exceeds the linewidth, the instability is described by quadratic dispersion Eq. (19) with solutions $k^{(1)}$ and $k^{(2)}$. Consequently, the electric field and the perturbation of the current density in the working zone are given by

$$E \sim c_1 \exp(ik^{(1)}z) + c_2 \exp(ik^{(2)}z), \quad (24)$$

$$\delta j_n \sim \frac{c_1}{\delta_1} \exp(ik^{(1)}z) + \frac{c_2}{\delta_2} \exp(ik^{(2)}z). \quad (25)$$

The coefficients

$$\delta_{1,2} = 1 - \frac{v_n}{\omega} k^{(1,2)} + \frac{\hbar}{2\omega} \frac{\partial^2 \varepsilon_n}{\partial p_n^2} k^{(1,2)2} \quad (26)$$

introduce deviations of the wave numbers $k^{(1)}$ and $k^{(2)}$ from the synchronism, and the coefficients c_i are determined from the boundary conditions as was discussed in Sec. III A. Using boundary conditions (21) and (22), we arrive at the linear system for c_i as follows:

$$c_1 + c_2 = \alpha [c_1 \exp(ik^{(1)}L) + c_2 \exp(ik^{(2)}L)],$$

$$\frac{c_1}{\delta_1} + \frac{c_2}{\delta_2} = 0. \quad (27)$$

Nontrivial solution of this system is determined by the equation

$$\delta_1 [1 - \alpha \exp(ik^{(1)}L)] - \delta_2 [1 - \alpha \exp(ik^{(2)}L)] = 0. \quad (28)$$

A current density satisfying Eq. (28) is the *threshold current density* of the generation. To evaluate this quantity, characteristic Eq. (28) must be solved together with Eq. (19). Substituting the roots

$$k^{(1,2)} = k_{m,\text{ch}} + \frac{b_{nn}^{(m)}}{\hbar v_n (k_{\text{ch}} - k'_m)} \quad (29)$$

of dispersion Eq. (19), with k_{ch} extracted from the synchronism condition $\omega - k_{\text{ch}} v_n + (\hbar k_{\text{ch}}^2 / 2) \partial^2 \varepsilon_n / \partial p_n^2 = 0$, into Eq. (28) and solving the resulting equation with respect to the current density, we obtain

$$\frac{b_{nn}^{(m)}}{\hbar v_n} L^2 \frac{\sin^2 x}{x^2} = 1 - |\alpha| + Lk_m'', \quad (30)$$

where

$$x = \left(\omega - k'_m v_n + \frac{\hbar k_m'^2}{2} \frac{\partial^2 \epsilon_n}{\partial p_n^2} \right) \frac{L}{2c} \quad (31)$$

is the dimensionless off-synchronism parameter.

Physically, Eq. (30) establishes the energy balance in the working zone. Its left-hand part determines the radiation production which is therefore proportional to the electron density n_e and to the squared interaction length. The factor $\sin^2 x/x^2$ determines the so-called gain curve—the gain dependence on the off-synchronism parameter x . In the case considered the gain curve is symmetrical with respect to $x=0$ and is maximal at zero deviation x . Further we compare this result with the classical case of small recoil and demonstrate significant difference in the behavior of gain curves. The term $1-\alpha$ in the right-hand part of Eq. (30) corresponds to the radiation leakage through the boundaries of the interaction zone while the last term specifies the radiation absorption by nanotube.

Energy balance Eq. (30) allows the evaluation of the threshold current density. If the current density in CNT exceeds the threshold value, the generation process is developed. The characteristic time of the instability development is inversely proportional to the *absolute instability increment* $\omega'' = \text{Im}(\omega)$, which is derived by solving generation Eq. (28) with respect to $\omega(k)$. In the low-gain regime,³⁹ which implies the conditions $|\Delta k''|L \ll 1$ and $1-\alpha \ll 1$ to be fulfilled, the increment is given by

$$\omega_m'' = \left[\frac{\partial k_m}{\partial \omega} \right]^{-1} \left(\frac{b_{nn}^{(m)}}{\hbar v_n} L \frac{\sin^2 x}{x^2} - \frac{1-|\alpha|}{L} - k_m'' \right). \quad (32)$$

In the linear stage of the radiative instability development, the electromagnetic field grows with time as $\exp(\omega_m'' t)$.

C. Starting current in the classical regime of interaction

In the case when quantum recoil can be neglected, dispersion Eq. (16) gives three roots

$$k^{(1)} = k_m - b_{nn}^{(m)} \frac{\partial^2 \epsilon_n}{\partial p_n^2} \frac{k_m'^2}{(\omega - v_n k_m')^2},$$

$$k^{(2,3)} = k_{\text{ch}} \pm \frac{i}{v_n} \sqrt{b_{nn}^{(m)} \frac{\partial^2 \epsilon_n}{\partial p_n^2} k_{\text{ch}}'^2 - k_m'^2}. \quad (33)$$

and, consequently, electromagnetic field in the interaction region is given by Eq. (23) with $N=3$. Correspondingly, perturbations of the electron and the current densities in the beam are written as

$$\delta j_n \sim \sum_{i=1}^3 \frac{c_i}{v_i^2}, \quad \delta j_n - v_n \delta n_e \sim \sum_{i=1}^3 \frac{c_i}{v_i}, \quad (34)$$

where deviations v_i are given by Eq. (26) with the last term omitted, i.e., $v_i = 1 - k^{(i)} v_n / \omega$. Then, by analogy with the previous section, we obtain the linear system

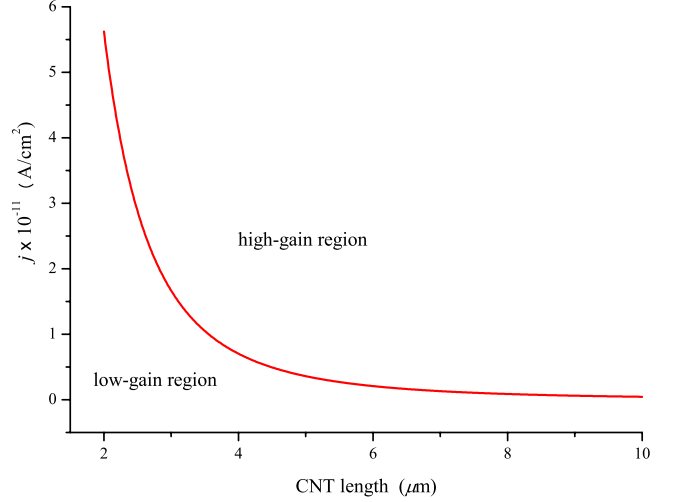


FIG. 1. (Color online) Demarcation between low-gain and high-gain regimes of generation Eq. (36).

$$c_1 + c_2 + c_3 = \alpha [c_1 \exp(ik^{(1)}L) + c_2 \exp(ik^{(2)}L) + c_3 \exp(ik^{(3)}L)],$$

$$\frac{c_1}{v_1} + \frac{c_2}{v_2} + \frac{c_3}{v_3} = 0,$$

$$\frac{c_1}{v_1^2} + \frac{c_2}{v_2^2} + \frac{c_3}{v_3^2} = 0, \quad (35)$$

and corresponding generation equation

$$v_1^2(v_2 - v_3)[1 - \alpha \exp(ik^{(1)}L)] - v_2^2(v_1 - v_3)[1 - \alpha \exp(ik^{(2)}L)] + v_3^2(v_1 - v_2)[1 - \alpha \exp(ik^{(3)}L)] = 0. \quad (36)$$

This equation we solve in the low-gain limit, which is determined by the condition $k_z'' L \leq 1$. The curve depicted in Fig. 1 divides out areas of parameters corresponding to low-gain and high-gain regimes, respectively. Then, solutions of Eq. (36)—the threshold current and the temporal instability increment—are given by

$$\frac{b_{nn}^{(m)}}{v_n^2} \frac{\partial^2 \epsilon_n}{\partial p_n^2} k L^3 \frac{x \cos x - \sin x}{x^3} = 1 - |\alpha| + Lk_m'', \quad (37)$$

$$\omega_m'' = \left[\frac{\partial k_m}{\partial \omega} \right]^{-1} \left[\frac{b_{nn}^{(m)}}{v_n^2} \frac{\partial^2 \epsilon_n}{\partial p_n^2} L^2 \frac{x \cos x - \sin x}{x^3} - \frac{1-|\alpha|}{L} + k_m'' \right]. \quad (38)$$

with the parameter x defined by Eq. (31). As follows from balance Eqs. (30) and (37), in the quantum interaction regime the radiation production per unit length is characterized by the linear dependence on L while this dependence becomes quadratic in the classical regime. Besides, the gain curves display distinctive behavior in these two cases. As different from the quantum interaction regime, in the classical limit the gain curve has asymmetrical character³⁹ due to

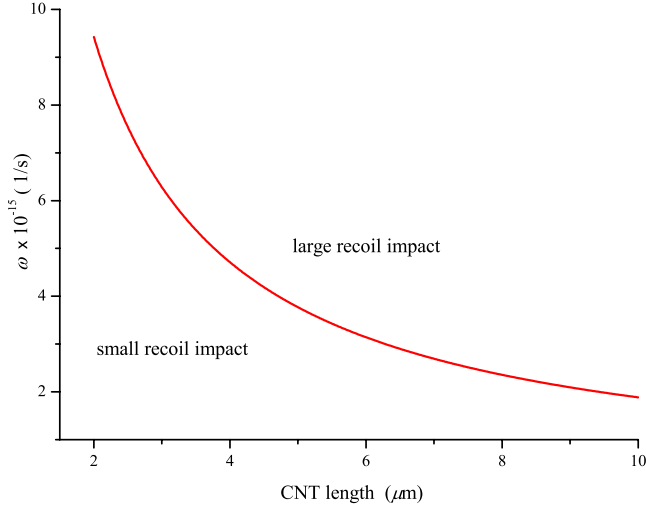


FIG. 2. (Color online) The curve divides the regions of parameters with small and large impacts of the quantum recoil on the generation. The curve has been obtained for the low-gain regime.

the interference of absorption and emission processes separated in this case by a frequency gap narrower than the linewidth. As a result, sign of the absolute instability increment depends on the sign of the synchronism detuning. At positive detuning the system is closer to the absorption frequency while negative detuning moves the system to the emission frequency.

Qualitatively, the classical and quantum interaction regimes are divided by the demarcation line depicted in Fig. 2. In the area above the line the quantum recoil at the generation must be taken into account while in the area below the line this effect can be ignored. The line course can easily be explained just by the increase in the photon energy with frequency. In addition, the increase in the generation length L leads to narrowing of the gain line and, as a result, the quantum recoil comes into play at smaller frequencies.

D. Role of electron spread

If electrons in the beam are distributed over a large number of energy levels and energy spread significantly exceeds the gap between emission and absorption lines, the total current is obtained by summation over this distribution. The generalization of Eq. (16) on this case is obvious:

$$k - k_m(\omega) = -b_{nn}^{(m)} \int dv f(v) \frac{\partial^2 \varepsilon_n}{\partial p_n^2} \frac{k^2}{(\omega - vk)^2}.$$

This equation can be rewritten in the form, conventional in plasma physics:⁵⁷

$$k - k_m(\omega) = b_{nn}^{(m)} k \frac{\partial^2 \varepsilon_n}{\partial p_n^2} \int \frac{\partial f(v)}{\partial v} \frac{dv}{\omega - vk + i0}. \quad (39)$$

Deriving Eq. (39) we assumed the dependence of the normalized distribution function $[\int f(v) dv = 1]$ on the group velocity to be narrower than corresponding dependences of the matrix element $b_{nn}^{(m)}$ and second derivative of the energy $\partial^2 \varepsilon_n / \partial p_n^2$. Then, considering the group-velocity spread ex-

ceeding the spontaneous emission linewidth, $\omega \Delta v / c \gg c / (\omega L)$, in Eq. (39) we can make use of the standard representation

$$\frac{1}{\omega - vk + i0} = \mathcal{P} \frac{1}{\omega - vk} - i\pi \delta(\omega - vk). \quad (40)$$

The principal value of the integral determines the real-valued component which is out of our interest.

If resonant interaction between electron beam and electromagnetic field occurs in the region of the negative derivative of the distribution function, i.e., $\partial f(v) / \partial v < 0$, then $k'' > 0$ and the generation process is not developed [we choose the $\exp(ikL)$ dependence]. This is because the majority of electrons in that case have velocities smaller than the resonant velocity and therefore they absorb the electromagnetic wave energy. Such a situation takes place in equilibrium, when the number of particles occupying energy level grow less with the level energy increase. In such a system, an initial perturbation attenuates. This process is commonly known as the Landau attenuation.

If the resonance is in the region with positive derivative $\partial f(v) / \partial v > 0$, the radiative instability is possible and obeys the condition

$$k_m'' - \pi b_{nn}^{(m)} \frac{\partial^2 \varepsilon_n}{\partial p_n^2} \left. \frac{\partial f(v)}{\partial v} \right|_{v=\omega/k} < 0, \quad (41)$$

which originates from the requirement $k'' < 0$ and from Eqs. (39) and (40). Condition (41) expresses the excess of emission over absorption. As one can see, the emission per unit length does not depend on the interaction length.

The imaginary part of the wave number k describes the asymptotic exponential behavior of the electromagnetic field in a continuous medium. To reach generation in a finite region, corresponding boundary conditions must be imposed. At a large spread, when the resonant term in Eq. (39) can be presented by Eq. (40), dispersion Eq. (39) has the only root. Using Eq. (22) we arrive at the relation $c_1 = \alpha \exp(ik^{(1)}L)c_1$, which dictates the generation equation as

$$1 - \alpha \exp(ik^{(1)}L) = 0. \quad (42)$$

For the Cherenkov radiation mechanism, solution of Eq. (42) leads to the equations as follows for the threshold current density and the absolute instability increment:

$$\pi b_{nn}^{(m)} \frac{\partial^2 \varepsilon_n}{\partial p_n^2} L \left. \frac{\partial f(v)}{\partial v} \right|_{v=\omega/k} = 1 - |\alpha| + L k_m'', \quad (43)$$

$$\omega_m'' = \left[\frac{\partial k_m'}{\partial \omega} \right]^{-1} \left[\pi b_{nn}^{(m)} \frac{\partial^2 \varepsilon_n}{\partial p_n^2} \left. \frac{\partial f(v)}{\partial v} \right|_{v=\omega/k} - \frac{1 - |\alpha|}{L} - k_m'' \right]. \quad (44)$$

Equation (44) shows that the production of stimulated radiation in the case of large spread is defined by the spread and falls down with its increase. The line dividing the range of parameters into two domains, with weak and strong influences of the energy spread, is depicted in Fig. 3. With the CNT length increase, the role of the spread also rises due to the gain line narrowing.

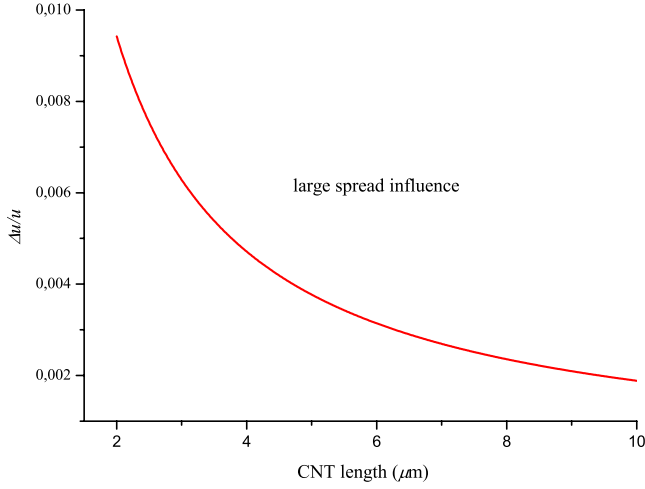


FIG. 3. (Color online) The regions of parameters with small (below curve) and strong (above the curve) influences of the electron-beam spread.

The extension of the obtained generation conditions to the case of interband transitions (i.e., to the undulator regime) is obvious and, in accordance with dispersion Eq. (15) for the undulator regime, is achieved by the substitution $\omega - kv_n \rightarrow \omega - kv_s - \Omega_{ns}$ in off-synchronism parameter (31), and the substitution $\hbar k^2 \partial^2 \epsilon_n / \partial p_n^2 \rightarrow \hbar k^2 \partial^2 \epsilon_s / \partial p_n^2 - 2\Omega_{ns}$ in expressions for threshold currents (30), (37), and (43), and for absolute instability increments (32), (38), and (44).

The analytics presented in this section implies fulfillment of several simplifying approximations: smallness of the photon momentum $\hbar k/p \ll 1$, small or large influence of the electron recoil on the emission (absorption), and small or large electron spread. Obviously, the analytical approaches do not work in intermediate cases; Eq. (12) supplemented by corresponding boundary conditions requires numerical integration. The number of roots of the dispersion equation to be accounted for and corresponding number of boundary conditions to be imposed is dictated by concrete physical parameters of the system being considered.

IV. PHYSICAL ANALYSIS AND NUMERICAL ESTIMATES

In Sec. II A it has been stated that classical treatment of electromagnetic field is valid if the field strength E_e amounts to a certain sufficiently large value. This value is determined by the condition imposed on the number of photons per energy level to exceed unity.⁵⁷ At the initial stage of the instability development, with less than one photon per energy level, the photon dynamics is described within the quantum electrodynamics formalism.

Usually, the number of photons per energy level is given by $n_{\text{ph}}(c/\omega)^3$, where n_{ph} is the photon number per unit volume while the quantity $(\omega/c)^3$ determines the number of photon levels lying below the energy $\hbar\omega$. As different from that, in the case of high-coherent laser radiation, the radiation is concentrated in a narrow spectral range $\Delta\omega \sim c/L$. As a result, the parameter defining the possibility of classical consideration of electromagnetic waves—the number of photons

per energy level—is derived as the density of the beam's kinetic energy converted to electromagnetic field divided by the photon energy and the number of levels below $\hbar\omega$. The ratio is found to be

$$\sim \eta_{\text{ph}} \frac{j}{ve} \left(\frac{c}{\omega} \right)^2 L \frac{k_m c}{\omega} \frac{mc^2(\gamma-1)}{\hbar\omega},$$

where j is the current density, v is the electron velocity, and η_{ph} is the efficiency of the transfer of electron kinetic energy to electromagnetic field. For infrared photons and electrons of several electron volt energy and $\sim 10 \mu\text{m}$ length nanotube, the photon number per energy level exceeds unity (i.e., the classical treatment is possible) if $\eta_{\text{ph}} > 10^{-5}$. Since the initial stage of the instability development is beyond the scope of our paper, the parameter η_{ph} can be estimated from the relation $\eta_{\text{ph}} \sim 1/(kL) \sim 0.02$, which corresponds to so-called nonlinear saturation regime³⁹ and determines the electron-beam energy conversion in saturation. Therefore, generation threshold and nonlinear stage of the instability development can be considered classically.

The simplest way to realize nano-FEL in carbon nanotube is to inject into it a high-energy external electron beam. Since the velocity of free electron is $v(\text{cm/s}) = 5.7 \times 10^7 \sqrt{\varphi(\text{eV})}$, in order to accelerate electrons up to velocities providing the synchronism regime (with 50–100 times wave slowing down predicted in Ref. 7), it is necessary to apply voltage of $\varphi \sim 7 \text{ eV}$. If the CNT diameter is such that its product with the electron transversal momentum is $p_{\perp} D / \hbar \sim 10\text{--}100$, the electron motion can be treated as classical. In that case, the term in the right part of dispersion Eq. (16) can be modified in the following way

$$b_{nm}^{(m)} \frac{\partial^2 \epsilon_n}{\partial p_n^2} \frac{k^2}{(\omega - v_n k)^2} \sim \omega_L^2 \frac{(\mathbf{v}\mathbf{e})^2}{2k'_m c^2} \frac{k^2}{(\omega - vk)^2}, \quad (45)$$

where \mathbf{v} is the classical electron velocity and \mathbf{e} is polarization vector for the electromagnetic mode considered. This simplification, after substitution of Eq. (45) into Eqs. (37) and (38), allows us to estimate the threshold current required to start the generation process and the instability increment, respectively. The dependences of these quantities on the CNT length are depicted in Figs. 4 and 5. Calculations have been done for $1 \mu\text{m}$ radiation wavelength and for the reflection coefficient from the working zone boundaries $\alpha = 0.99$. Generation in the terahertz range would require higher current density. It follows from Fig. 5 that the gain for CNT is extremely large as compared with macroscopic electronic devices. For chosen parameters, the generation development starts when the CNT length is about $6 \mu\text{m}$ or larger, which is technologically routine range. Therefore, our calculations demonstrate that the development of CNT-based nano-FEL is already possible at the current stage of nanotechnology. The characteristic time of the instability evolution is inversely proportional to the instability increment and, for $10 \mu\text{m}$ nanotube, is a fraction of nanosecond.

A positive feedback is required for the realization of oscillator regime; reflection from CNT ends¹⁰ can serve as a possible mechanism of the feedback. The reflection can be intensified by variation in the CNT generic parameters,

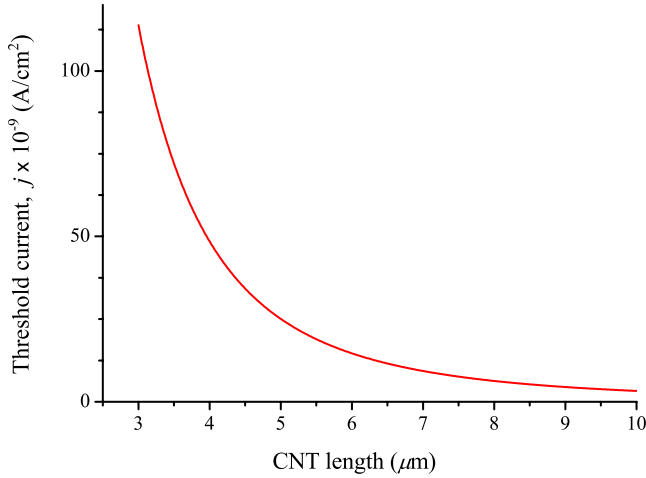


FIG. 4. (Color online) The dependence of threshold current density on nanotube length.

proper selection of surrounding medium, and using other methods commonly applied in laser physics and electronics. An alternative mechanism providing the feedback is excitation of backward modes propagating oppositely to electron flow. The backward modes are possible because CNTs are periodic along their axis and, consequently, their eigenmodes are Bloch modes containing waves with both positive and negative phase velocities. As a result, there exist Bloch modes with group velocity directed oppositely to the electron velocity—the backward modes.⁴⁰ One of the waves of the backward mode having a positive phase velocity can be synchronized with the electron flow. In this case the positive feedback is provided automatically.

The instability process is developed only if the electron free-path length is comparable or even exceeds the working zone length, i.e., the electron motion is ballistic within the zone. Otherwise, random collisions of electrons cause a phase shift which prevents the electron flow bunching and breaks the radiation coherence. As was mentioned above, in metallic single-walled CNTs the free-path length is about several microns.⁵⁰⁻⁵² A longer ballisticity area can be provided by proper external conditions. For example, in a regular array of oriented nanotubes the suppression of electron

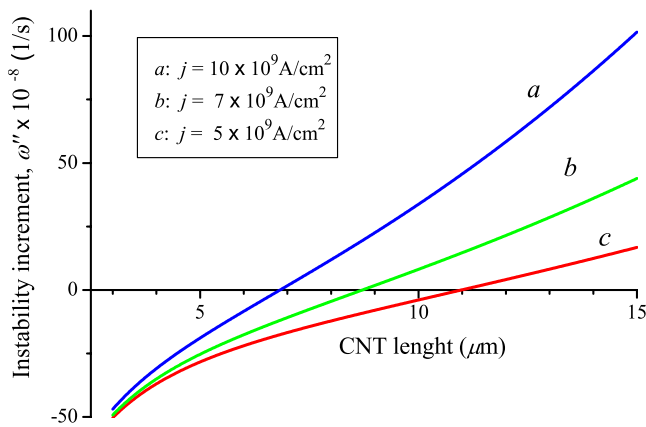


FIG. 5. (Color online) Instability increment vs nanotube length at different electron current densities.

collisions with atoms can be achieved using the properties of the electron diffraction in periodical structures. In a densely packed array of CNTs—CNT bundle—nanotubes form a lattice with the distance between CNTs' axes $2R_{cn}+d$, where $d \approx 3.2 \text{ \AA}$ is the interlayer distance in graphite. Correspondingly, the reciprocal-lattice vector in such a lattice has the value $h=2\pi/(2R_{cn}+d)$. From the principle of uncertainty we can estimate the transverse component of the momentum by $p_{\perp}/\hbar \sim 2\pi/2R_{cn}$. Obviously, the Bragg condition $|\mathbf{p}_{\perp}+\mathbf{h}| \approx |\mathbf{p}_{\perp}|$ can be fulfilled for a large portion of electrons passing the bundle and six-wave diffraction⁶⁰ can be realized. Owing to the diffraction, electrons are concentrated in domains free of atoms and, therefore, scattering is weak for such electrons. Analogous situation meet in the Bormann effect⁶⁰ for hard x rays passing through a crystal. Owing to this effect, a significant increase in the photon free path is observed. The increase in the electron free-path results in the increase in the generation length L and, consequently, in the strong decrease in the threshold current. Thus, the use of CNT bundles instead of isolated single-walled CNTs is a rote to retain ballistical regime of the electron motion at required values of the threshold current. Even if generation conditions are provided by the use of external electron beam, the idea to exploit intrinsic electrons of CNTs looks very attractive because it would solve the dramatic problem of focusing an external electron beam into a spot of the CNT diameter size. Typical velocity of π electrons excited to energy of several electron volts is about $3 \cdot 10^8 \text{ cm/s}$. For such electrons, the synchronism condition requires the electromagnetic wave slowing down as large as 300 times, which is much larger than the theoretical estimate⁷ gives for CNTs.

In such a situation, special configurations providing higher group velocity are extremely desirable; otherwise, stronger excitation of electrons is necessary to fulfill the Cherenkov generation condition. Fortunately, as compared to vacuum electronic devices, stimulated emission in CNTs features a set of new promising properties. In macroscopic Cherenkov FELs the electron energy ordinarily rises with the electron velocity and, in nonrelativistic regime, quadratically depends on the momentum (and velocity). As a result, the only way to reach the synchronism condition in that case is to increase the electron-beam energy. For a collective (quasi) electrons in CNT, such is not the case. Indeed, the electron group velocity, which is analog of the velocity for quasiparticles, is determined by the properties of the whole system and may demonstrate nontrivial dependence on the quasimomentum. Locally, the quasiparticle velocity may recede as energy rises. Correspondingly, local maxima of the group velocity may appear. If one seeks the synchronism condition for a low-energy quasiparticle, it is advantageous to choose parameters in the vicinity of the group velocity local maxima. It allows attaining the synchronism in a relatively low accelerating potential and, therefore, significantly reduces the CNT energy load.

Let us exemplify the statement considering an isolated straight (q, q) armchair CNT. The dispersion law of π electrons in such a CNT is given by²

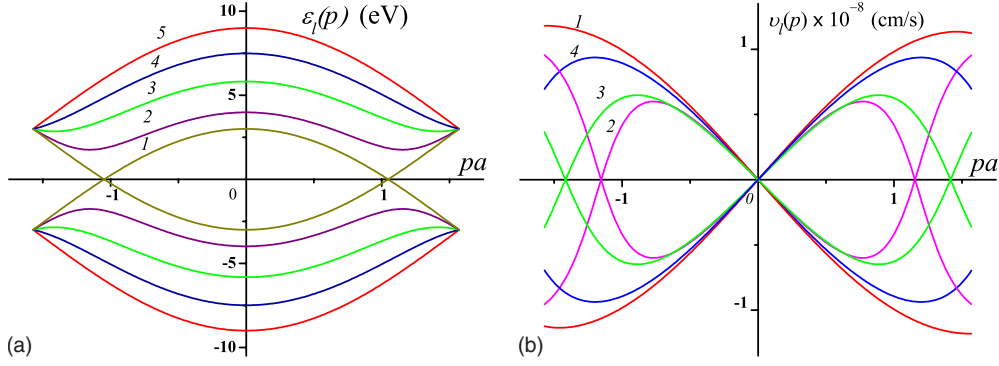


FIG. 6. (Color online) (a) Energy and (b) group velocity vs quasimomentum for (10,10) armchair nanotube. The numbers near the curves numerate different modes.

$$\varepsilon_l(p) = \mp \gamma_0 [1 \pm 4 \cos(\pi l/q) \cos(pa) + 4 \cos^2(pa)]^{1/2}, \quad (46)$$

where $\gamma_0 \approx 2.7$ eV is the overlap integral, $l=1, \dots, 2q$, $a = \sqrt{3}b/2\hbar$, and $b=1.42$ Å is the interatomic distance in graphite. The upper and lower signs refer to the conduction and valence bands, respectively. The group velocity corresponding to this law is

$$v_l = \mp 2\gamma_0 a \sin(pa) \times \frac{\mp \cos(\pi l/q) - 2 \cos(pa)}{[1 \pm 4 \cos(\pi l/q) \cos(pa) + 4 \cos^2(pa)]^{1/2}}. \quad (47)$$

Calculations of the energy and the group velocity for (10,10) nanotube by Eqs. (46) and (47) are presented in Fig. 6. The curves in two figures can easily be correlated: The larger slope of the dispersion curve the larger the group velocity. Typical velocity of π electrons excited to energy of several electron volts is about $3 \cdot 10^8$ cm/s. For such electrons, the synchronism condition requires the electromagnetic wave slowing down as large as 300 times. A proper choice of the excited state in the vicinity of the group-velocity local maximums allows essential weakening of this restriction.

The region in the vicinity of the group-velocity extremum is also attractive because of the weak velocity dependence on the quasimomentum. As a result, in this region irradiation of photon gets the electron only slightly out of the synchronism condition keeping high the probability to emit next photon. Due to that, the radiation effectiveness grows in the vicinity of the group-velocity extremum. An additional advantage of the local maximum in the group velocity is the smaller negative influence of the beam energy spread on the generation effectiveness. Indeed, in the vicinity of the group-velocity extremum, the Taylor expansion of the energy does not contain linear quasimomentum terms. As a result, a larger number of particles in a spreaded beam appear to be synchronized with electromagnetic wave. This effect is characteristic for quasiparticles and fully absent for free electrons.

The effect of radiation instability in nanotube can be controlled by the variation in the electron effective mass. The smaller the mass the more responsive the electron is to perturbation, and the more likely an electron-beam bunching occurs. This means faster development of the instability. The

reciprocal electron effective mass is given by the quantity $\partial^2 \varepsilon_n / \partial p_n^2$, therefore, the increase in the instability increment as the effective mass grows smaller follows immediately from dispersion Eqs. (16) and (39), which involve the reciprocal mass.

One more mechanism, which does not require large wave slowing down, is exploiting electron interband transitions. In this case, as follows from Eq. (15), the resonance condition is $\omega - v_s k = \Omega_{ns}$ (we suppose that transition frequency exceeds the term related to the recoil) and the radiation frequency can vary from infrared to ultraviolet. For interband transitions, single-particle spontaneous emission of electron (positron) beams emerging from outside into nanotube was considered by Artru *et al.*²¹

In order to weaken the requirement imposed on the electromagnetic wave to be slowed down to the electron velocity, one can utilize the photon diffraction on a periodic lattice of carbon atoms in a nanotube. Resonance interaction takes place for harmonics corresponding to the reciprocal vector τ satisfying the condition $\omega - v_n(k + \tau) = 0$. Then, taking into account the condition $v_n/c \ll 1$, one can obtain

$$\omega_\tau = \frac{\tau v_n}{1 - n_{\text{ref}} v_n / c}. \quad (48)$$

Here $n_{\text{ref}} = kc/\omega$ is the effective refractive index of corresponding mode. The spatial period of a nanotube varies in wide range. For zigzag and armchair nanotubes, it is equal to 2.49 Å while for chiral nanotubes the translation period achieves 10 nm and more depending on the nanotube indices. As a result, the generated wavelength varies from ultraviolet (for armchair and zigzag CNTs) to infrared range for nanotubes with translation period $\sim 2\sqrt{3}\pi R_{\text{cn}}$.

V. CONCLUSION

In the present paper, aiming at the development of the physical basis of a unique class of nanosized light sources, we have investigated theoretically a recently proposed mechanism of the generation of stimulated electromagnetic radiation by electron beam in carbon nanotubes. The basic idea exploits an analogy between CNTs and macroscopic electron devices and utilizes the effect of wave slowing down in waveguides. Three basic properties of carbon nano-

tubes: the strong slowing down of surface electromagnetic waves, the ballistics of the electron motion over typical CNT length, and the extremely high electron current density reachable in CNTs, allow proposition of them as candidates for the development of nanoscale Cherenkov-type emitters for a wide frequency range from terahertz to optical. The threshold conditions evaluated from the theoretical model demonstrate that the development of CNT-based nano-FEL is already feasible at realistic present-day parameters of nanotubes. The use of CNT bundles is proposed as a means to decrease the threshold current density. Currently, we explore the possibility of reducing the generation voltage by the use of multiwalled CNTs, where electromagnetic modes exist⁶¹

with phase velocity essentially less than that predicted for single-walled CNTs.⁷ Generation on such a mode requires much less bias since $U \sim v_{ph}^2$. Detail analysis will be published elsewhere.

ACKNOWLEDGMENTS

The research was partially supported by the INTAS through Project No. 05-1000008-7801, the EU FP7 TerACan through Project No. FP7-230778, the IB BMBF (Germany) through Project No. BLR 08/001, and the Belarus Republican Foundation for Fundamental Research through Project No. F08R-009.

-
- ¹S. Iijima, *Nature (London)* **354**, 56 (1991).
²M. S. Dresselhaus, G. Dresselhaus, and Ph. Avouris, *Carbon Nanotubes* (Springer, Berlin, 2001).
³S. Reich, C. Thomsen, and J. Maultzsch, *Carbon Nanotubes, Basic Concepts and Physical Properties* (Wiley-VCH, Berlin, 2004).
⁴P. G. Collins and Ph. Avouris, *Sci. Am.* **12**, 62 (2000).
⁵L. Novotny and B. Hecht, *Principles of Nano-Optics* (Cambridge University Press, Cambridge, 2006).
⁶P. Longe and S. M. Bose, *Phys. Rev. B* **48**, 18239 (1993).
⁷G. Ya. Slepyan, S. A. Maksimenko, A. Lakhtakia, O. Yevtushenko, and A. V. Gusakov, *Phys. Rev. B* **60**, 17136 (1999).
⁸S. A. Maksimenko and G. Ya. Slepyan, in *The Handbook of Nanotechnology: Nanometer Structure Theory, Modeling, and Simulation*, edited by A. Lakhtakia (SPIE, Bellingham, 2004), p. 145.
⁹G. W. Hanson, *IEEE Trans. Antennas Propag.* **53**, 3426 (2005).
¹⁰G. Ya. Slepyan, M. V. Shuba, S. A. Maksimenko, and A. Lakhtakia, *Phys. Rev. B* **73**, 195416 (2006).
¹¹P. J. Burke, S. Li, and Z. Yu, *IEEE Trans. Nanotechnol.* **5**, 314 (2006).
¹²K. Kempa, J. Rybczynski, Z. Huang, K. Gregorczyk, A. Vidan, B. Kimball, J. Carlson, G. Benham, Y. Wang, A. Herczynski, and Z. F. Ren, *Adv. Mater. (Weinheim, Ger.)* **19**, 421 (2007).
¹³M. V. Shuba, S. A. Maksimenko, and A. Lakhtakia, *Phys. Rev. B* **76**, 155407 (2007).
¹⁴I. V. Bondarev, G. Ya. Slepyan, and S. A. Maksimenko, *Phys. Rev. Lett.* **89**, 115504 (2002).
¹⁵A. M. Nemilentsau, G. Ya. Slepyan, and S. A. Maksimenko, *Phys. Rev. Lett.* **99**, 147403 (2007).
¹⁶A. Hartschuh, E. J. Sanchez, X. S. Xie, and L. Novotny, *Phys. Rev. Lett.* **90**, 095503 (2003).
¹⁷A. Hartschuh, H. Qian, A. J. Meixner, N. Anderson, and L. Novotny, *J. Lumin.* **119-120**, 204 (2006).
¹⁸Y. Wang, K. Kempa, B. Kimball, G. Benham, W. Z. Li, T. Kempa, J. Rybczynski, A. Herczynski, and Z. F. Ren, *Appl. Phys. Lett.* **85**, 2607 (2004).
¹⁹J. Rybczynski, K. Kempa, A. Herczynski, Y. Wang, M. J. Naughton, Z. F. Ren, Z. P. Huang, D. Cai, and M. Giersig, *Appl. Phys. Lett.* **90**, 021104 (2007).
²⁰V. V. Klimov and V. S. Letokhov, *Phys. Lett. A* **222**, 424 (1996).
²¹X. Artru, S. P. Fomin, N. F. Shul'ga, K. A. Ispirian, and N. K. Zhevago, *Phys. Rep.* **412**, 89 (2005).
²²S. Bellucci, *Nucl. Instrum. Methods Phys. Res. B* **234**, 57 (2005).
²³J. A. Misewich, R. Martel, Ph. Avouris, J. C. Tsang, S. Heinze, and J. Tersoff, *Science* **300**, 783 (2003).
²⁴J. Chen, V. Perebeinos, M. Freitag, J. Tsang, Q. Fu, J. Liu, and P. Avouris, *Science* **310**, 1171 (2005).
²⁵D. Dragoman and M. Dragoman, *Prog. Quantum Electron.* **28**, 1 (2004).
²⁶O. V. Kibis, D. G. W. Parfitt, and M. E. Portnoi, *Phys. Rev. B* **71**, 035411 (2005).
²⁷O. V. Kibis, S. V. Malevanny, L. Hugget, D. G. W. Parfitt, and M. E. Portnoi, *Electromagnetics* **25**, 425 (2005).
²⁸O. V. Kibis and M. E. Portnoi, *Tech. Phys. Lett.* **31**, 671 (2005).
²⁹O. V. Kibis, M. Rosenau da Costa, and M. E. Portnoi, *Nano Lett.* **7**, 3414 (2007).
³⁰M. E. Portnoi, O. V. Kibis, and M. Rosenau da Costa, *Superlattices Microstruct.* **43**, 399 (2008).
³¹K. G. Batrakov, P. P. Kuzhir, and S. A. Maksimenko, *Proc. SPIE* **6328**, 63280Z (2006).
³²P. Kuzhir, K. Batrakov, and S. Maksimenko, *Synth. Reactivity Inorg., Metal-Organ., Nano-Metal Chemistry* **37**, 341 (2007).
³³K. G. Batrakov, P. P. Kuzhir, and S. A. Maksimenko, *Physica E (Amsterdam)* **40**, 1065 (2008).
³⁴K. G. Batrakov, P. P. Kuzhir, and S. A. Maksimenko, *Physica E (Amsterdam)* **40**, 2370 (2008).
³⁵R. Varian and S. Varian, *J. Appl. Phys.* **10**, 321 (1939).
³⁶R. Kompfner, *The Invention of the Travelling Wave Tube* (San Francisco, San Francisco, 1964).
³⁷J. M. J. Madey, *J. Appl. Phys.* **42**, 1906 (1971).
³⁸F. A. Hopf, P. Meystre, M. O. Scully, and W. H. Louisell, *Phys. Rev. Lett.* **37**, 1215 (1976).
³⁹T. C. Marshall, *Free Electron Lasers* (Macmillan, New York, 1985).
⁴⁰E. L. Saldin, E. A. Schneidmiller, and M. V. Yurkov, *The Physics of Free Electron Lasers* (Springer-Verlag, Berlin, 2000).
⁴¹SLAC Report No. SLAC-R-593, 2002 (unpublished).
⁴²DESY Report No. DESY 2006-097, 2006 (unpublished); see also URL <http://xfel.desy.de>.
⁴³S. J. Smith and E. M. Purcell, *Phys. Rev.* **92**, 1069 (1953).
⁴⁴V. Baryshevsky, K. Batrakov, and I. Dubovskaya, *J. Phys. D* **24**, 1250 (1991).

- ⁴⁵R. Q. Twiss, *Aust. J. Phys.* **11**, 564 (1958).
- ⁴⁶J. Schneider, *Phys. Rev. Lett.* **2**, 504 (1959).
- ⁴⁷V. G. Baryshevsky and I. D. Feranchuk, *Phys. Lett.* **102**, 141 (1984).
- ⁴⁸A. Friedman, A. Gover, G. Kurizki, S. Ruschin, and A. Yariv, *Rev. Mod. Phys.* **60**, 471 (1988).
- ⁴⁹R. B. Miller, *An Introduction to the Physics of Intense Charged Particles Beams* (Plenum, New York, 1982).
- ⁵⁰S. Frank, P. Poncharal, Z. L. Wang, and W. A. de Heer, *Science* **280**, 1744 (1998).
- ⁵¹C. Berger, Y. Yi, Z. L. Wang, and W. A. de Heer, *Appl. Phys. A: Mater. Sci. Process.* **74**, 363 (2002).
- ⁵²C. Berger, P. Poncharal, Y. Yi, and W. A. de Heer, *J. Nanosci. Nanotechnol.* **3**, 171 (2003).
- ⁵³Z. Yao, C. L. Kane, and C. Dekker, *Phys. Rev. Lett.* **84**, 2941 (2000).
- ⁵⁴B. Q. Wei, R. Vajtai, and P. M. Ajayan, *Appl. Phys. Lett.* **79**, 1172 (2001).
- ⁵⁵R. Vajtai, B. Q. Wei, Z. J. Zhang, Y. Jung, G. Ramanath, and P. M. Ajayan, *Smart Mater. Struct.* **11**, 691 (2002).
- ⁵⁶V. B. Berestetskii, E. M. Lifshitz, and L. P. Pitaevskii, *Quantum Electrodynamics* (Pergamon, Oxford, 1982).
- ⁵⁷L. D. Landau and E. M. Lifshitz, *Quantum Mechanics: Non-Relativistic Theory* (Pergamon, Oxford, 1977).
- ⁵⁸E. M. Lifshitz and L. P. Pitaevskii, *Physical Kinetics* (Pergamon, Oxford, 1981).
- ⁵⁹O. Zvelto, *Principles of Lasers* (Plenum, New York, 2004).
- ⁶⁰Shi-Lin Chang, *Multiple Diffraction of X-Rays in Crystals* (Springer-Verlag, Berlin, 1984).
- ⁶¹M. V. Shuba, G. Ya. Slepian, S. A. Maksimenko, A. Lakhtakia, and C. Thomsen, arXiv:0806.2958 (unpublished).